Vol 464|11 March 2010|doi:10.1038/nature08876

LETTERS

Transmission of electrical signals by spin-wave interconversion in a magnetic insulator

Y. Kajiwara[1,2], K. Harii[1], S. Takahashi[1,3], J. Ohe[1,3], K. Uchida[1], M. Mizuguchi[1], H. Umezawa[5], H. Kawai[5], K. Ando[1,2], K. Takanashi[1], S. Maekawa[1,3] & E. Saitoh[1,2,4]

The energy bandgap of an insulator is large enough to prevent electron excitation and electrical conduction[1]. But in addition to charge, an electron also has spin[2], and the collective motion of spin can propagate—and so transfer a signal—in some insulators[3]. This motion is called a spin wave and is usually excited using magnetic fields. Here we show that a spin wave in an insulator can be generated and detected using spin-Hall effects, which enable the direct conversion of an electric signal into a spin wave, and its subsequent transmission through (and recovery from) an insulator over macroscopic distances. First, we show evidence for the transfer of spin angular momentum between an insulator magnet $Y_3Fe_5O_{12}$ and a platinum film. This transfer allows direct conversion of an electric current in the platinum film to a spin wave in the $Y_3Fe_5O_{12}$ via spin-Hall effects[4–11]. Second, making use of the transfer in a Pt/$Y_3Fe_5O_{12}$/Pt system, we demonstrate that an electric current in one metal film induces voltage in the other, far distant, metal film. Specifically, the applied electric current is converted into spin angular momentum owing to the spin-Hall effect[7,8,10,11] in the first platinum film; the angular momentum is then carried by a spin wave in the insulating $Y_3Fe_5O_{12}$ layer; at the distant platinum film, the spin angular momentum of the spin wave is converted back to an electric voltage. This effect can be switched on and off using a magnetic field. Weak spin damping[3] in $Y_3Fe_5O_{12}$ is responsible for its transparency for the transmission of spin angular momentum. This hybrid electrical transmission method potentially offers a means of innovative signal delivery in electrical circuits and devices.

A flow of spin angular momentum is called a spin current[2]. In solids, there are two types of carriers for non-equilibrium spin currents. One is a conduction electron[2,12,13] (Fig. 1a). The other is collective motion of magnetic moments (Fig. 1b)—spin waves[14,15], comprising magnetostatic and exchange spin-wave modes[14,15]. Here we call a spin current carried by spin waves a 'spin-wave spin current' (see Supplementary Information section A for details).

Extensive studies of conduction-electron spin currents in metals and semiconductors have clarified that the currents have a critical problem; they disappear within a very short distance, typically hundreds of nanometres[16]. In contrast, it has been shown that a spin-wave spin current may persist for much greater distances because it is carried by the collective motion of spins coupled by exchange interaction[14,15]. Significantly, a spin-wave spin current exists even in magnetic insulators, in which its decay is typically suppressed. This is because the decay is caused mainly by conduction electrons, which are absent in insulators. For instance, in the magnetic insulator $Y_3Fe_5O_{12}$, the spin-wave decay length can be several centimetres[3] and thus the waves are propagated over a relatively long distance; $Y_3Fe_5O_{12}$ is an ideal conductor for spin-wave spin currents even though it is an insulator for electric currents.

To make use of the spin-wave spin currents in insulators, it is necessary to find methods for getting a d.c. spin current into and out of the insulators. We show that this can be done by using spin pumping and spin-transfer torque (STT). Here, spin pumping refers to the transfer of spin angular momentum from magnetization-precession motion to conduction-electron spin[9,17–19], a phenomenon

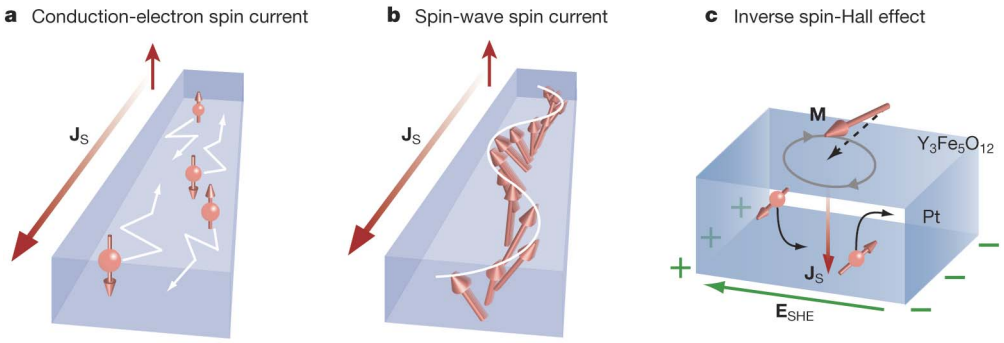

Figure 1 | Two types of non-equilibrium spin currents in solids. **a**, A schematic illustration of a conduction-electron spin current: spin angular momentum $\mathbf{J}_S$ carried by electron diffusion. **b**, A schematic illustration of a spin-wave spin current: spin angular momentum carried by collective magnetic-moment precession. **c**, A schematic illustration of the spin-pumping detection mechanism in the present system. If the magnetization ($\mathbf{M}$) dynamics in the $Y_3Fe_5O_{12}$ layer (on the top face of the block) pumps a spin current $\mathbf{J}_S$ into the Pt layer, the current generates electromotive force $\mathbf{E}_{SHE}$ via ISHE.

[1]Institute for Materials Research, Tohoku University, Sendai 980-8577, Japan. [2]Department of Applied Physics and Physico-Informatics, Keio University, Yokohama 223-8522, Japan. [3]CREST, [4]PRESTO, Japan Science and Technology Agency, Sanbancho, Tokyo 102-0075, Japan. [5]FDK Corporation, Shizuoka 431-0495, Japan.

which allows generation of a spin current from magnetization motion. STT is, in contrast, the reverse process of this spin pumping, that is, the transfer of angular momentum from conduction-electron spin to magnetization[20–22]: the magnetization receives torque by absorbing a spin current[20–22]. These two phenomena enable the mutual conversion of angular momentum between conduction-electron spin and magnetization. However, up to now, experiments on these phenomena have been limited to electric conductors. In this Letter we show that by using Pt/$Y_3Fe_5O_{12}$ films, both phenomena[23] occur even at insulator/metal interfaces, and the phenomena allow transmission of a d.c. electric signal through the insulator for a long distance in a controllable manner at room temperature.

First, we show evidence for spin pumping across a Pt/garnet-type $Y_3Fe_5O_{12}$ interface. $Y_3Fe_5O_{12}$ is a ferrimagnetic insulator whose charge gap is 2.7 eV. Owing to this huge gap, $Y_3Fe_5O_{12}$ exhibits very high resistivity ($\sim 10^{12}\,\Omega$ cm at room temperature, greater than that of air). Also, the magnetization damping is very small: $\alpha \approx 6.7 \times 10^{-5}$, where α is the Gilbert damping coefficient[19,24] for the sample used in the present study (Fig. 2b). Figure 2a is a schematic illustration of the experimental set-up. The sample is a bilayer film composed of a single-crystal $Y_3Fe_5O_{12}$ layer and a Pt layer. Here, the Pt layer is used as a spin-current detector, in which the inverse spin-Hall effect[9–11] (ISHE) converts a spin current into electromotive force $\mathbf{E}_{SHE}$ via the spin–orbit interaction. In ISHE, when a spin current carries the spin polarization $\boldsymbol{\sigma}$ along the spatial direction $\mathbf{J}_S$, $\mathbf{E}_{SHE}$ is given by[9,11] (Fig. 1c):

$$\mathbf{E}_{SHE} /\!/ \mathbf{J}_S \times \boldsymbol{\sigma} \quad (1)$$

ISHE is known to be enhanced in heavy noble metals such as Pt (refs 9, 11).

During the measurements, a static in-plane magnetic field H is applied and the sample is placed at the centre of a 9.44 GHz microwave cavity. When H fulfils the ferromagnetic spin-wave resonance (SWR) conditions[14,15], precession of magnetization is induced. If this precession pumps spin currents into the Pt layer, then voltage is generated in the Pt layer via ISHE; spin pumping in this system is sensitively detected by measuring the voltage difference V between the ends of the Pt layer[9,11].

Figures 2c and 2d are the SWR spectrum and the H dependence of dV/dH, respectively, both measured with microwaves applied and with the external magnetic field perpendicular ($\theta = 90°$) to the direction across the electrodes. In the SWR spectrum, many resonance signals appear, each dispersion corresponding to a SWR mode[14,15] in the $Y_3Fe_5O_{12}$ layer. These resonance fields are much greater than the in-plane magnetization saturation field ($H_C = 20$ Oe) of this $Y_3Fe_5O_{12}$ film. In the dV/dH spectrum, as shown in Fig. 2d, multiple peaks appear at these SWR fields, indicating that electromotive force is induced in the Pt layer concomitant with SWR in the $Y_3Fe_5O_{12}$ layer. Figure 2g shows the microwave-power dependence of the maximum peak values V_{max} in the $V(H)$ curves. The experimental data (filled circles) are well reproduced by a curve (solid line) calculated from a longitudinal spin-pumping model in which the spin accumulation in the Pt layer is taken into consideration (see Supplementary Information section B for details). This voltage signal was found to disappear in a Cu/$Y_3Fe_5O_{12}$ system, where the Pt layer is replaced by a Cu layer in which the spin–orbit interaction is very weak[22], indicating the important role of spin–orbit interaction, or ISHE, in the voltage generation. The voltage signal also disappears in a Pt/SiO_2/$Y_3Fe_5O_{12}$ system, where the $Y_3Fe_5O_{12}$ and the Pt layers are separated by a thin (10 nm) film of insulating SiO_2, and also in a Pt/$Gd_3Ga_5O_{12}$ system, where the $Y_3Fe_5O_{12}$ layer is replaced by a paramagnetic $Gd_3Ga_5O_{12}$ layer. These last two results indicate that direct contact between the magnet $Y_3Fe_5O_{12}$ and Pt is necessary for the observed voltage generation; electromagnetic artefacts are irrelevant. By changing the field direction θ, the V signal for Pt/$Y_3Fe_5O_{12}$ disappears at $\theta = 0$ (Fig. 2e, f) and then changes its sign at $-90° < \theta < 0$. This behaviour is consistent with equation (1), and is direct evidence for ISHE induced by spin pumping from the insulator $Y_3Fe_5O_{12}$.

The spin pumping in Pt/$Y_3Fe_5O_{12}$ can be attributed to the small but finite spin-exchange interaction[17,19] between a conduction electron in Pt and a localized moment in $Y_3Fe_5O_{12}$, or to the mixing conductance of the conduction electrons[23] at the interface. By taking this interaction into account in coupled equations for the magnetization and spin accumulation (the Landau–Lifshitz–Gilbert equation[24] and the Bloch equation with spin diffusion[17,19]), we obtain the pumped spin current, which when combined with ISHE[9–11] allows calculation of V as a function of the spin-exchange interaction at the interface. From the experimental values of V together with values of microwave field strength and the spin-Hall angle for Pt (ref. 11), the magnitude of the spin-exchange energy density at the interface is estimated to be $\sim 16\,\mathrm{erg\,cm^{-2}}$; alternatively, the magnitude of the mixing conductance[23] is estimated as $3 \times 10^{12}\,\mathrm{cm^{-2}}$ (see Supplementary Information section B for details).

The above observation of the spin pumping in Pt/$Y_3Fe_5O_{12}$ suggests the possibility of the reverse process: STT[20–22] acting on the insulator $Y_3Fe_5O_{12}$. Second, we demonstrate STT across the Pt/$Y_3Fe_5O_{12}$ interface using the same system as follows. We applied an

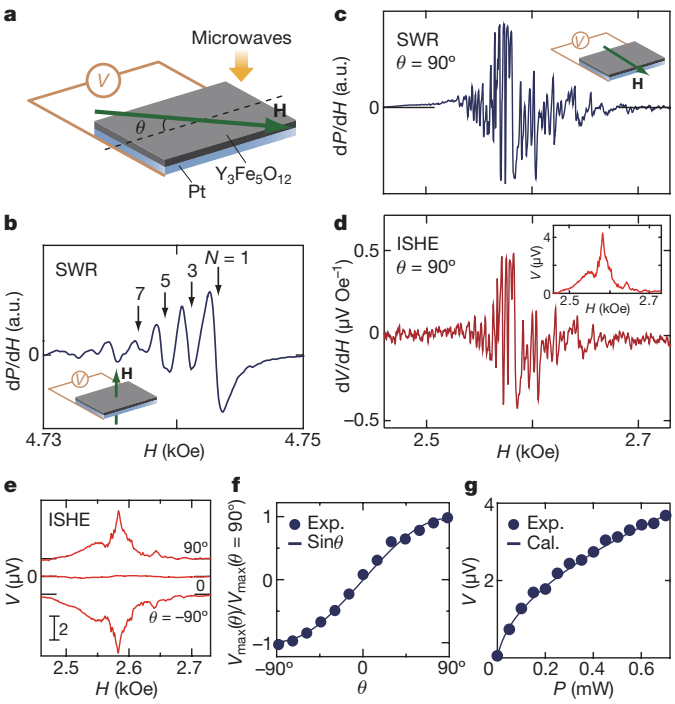

Figure 2 | Spin pumping in Pt/$Y_3Fe_5O_{12}$. **a**, Schematic illustration of the experimental set-up. The sample is a Pt/$Y_3Fe_5O_{12}$ bilayer film, 3 mm × 1 mm, composed of a 1.3-μm-thick garnet-type $Y_3Fe_5O_{12}$ layer and a 10-nm-thick Pt layer. The voltage (V) electrodes attached to the Pt film are 3 mm apart. **H** denotes the in-plane external magnetic field. **b**, SWR spectrum measured when a magnetic field is perpendicular to the film. Arrows, fitting results for the exchange spin-wave resonance fields[29]. N, spin-wave mode number along the direction perpendicular to the film. Spectral width and α for the $N = 1$ mode was estimated via a fitting procedure using Lorentz-type dispersion functions (Supplementary Information section E). P and H, the microwave absorption intensity and the strength of **H**, respectively. **c**, Ferromagnetic SWR spectrum for the Pt/$Y_3Fe_5O_{12}$ film at $\theta = 90°$ (θ is defined in **a**). **d**, H dependence of dV/dH for the Pt/$Y_3Fe_5O_{12}$ film measured by applying 1 mW microwaves at $\theta = 90°$. Inset, H dependence of V for the Pt/$Y_3Fe_5O_{12}$ film at $\theta = 90°$. Galvanomagnetic effects[24] in magnets are irrelevant to V, as $Y_3Fe_5O_{12}$ is an insulator. **e**, H dependence of V measured by applying the microwaves at various values of θ. **f**, θ dependence of the maximum peak values V_{max} in the $V(H)$ curves measured with application of microwaves. **g**, Microwave-power dependence of V_{max}. The experimental data (filled circles) are well reproduced by a curve (solid line) calculated from a longitudinal spin-pumping model.

electric current **J** to the Pt layer (Fig. 3a). In the Pt layer, **J** is converted into a spin current via the spin-Hall effect[7,8,11,22]. This spin current exerts STT on the magnetization in the $Y_3Fe_5O_{12}$ layer. This is the reverse process of the aforementioned spin pumping effect. When $J>0$ ($J<0$) at $\theta=90°$ ($\theta=-90°$), STT is antiparallel to the magnetization damping torque in the $Y_3Fe_5O_{12}$ layer[22] (Fig. 3b). Here, θ represents the angle between **J** and the magnetization direction of the $Y_3Fe_5O_{12}$ layer. In this case, if the magnitude of STT is greater than that of the damping torque, the damping is cancelled out by STT. This means that when a sufficient amount of current is applied, the magnetization spontaneously oscillates[20–22] with the eigenfrequencies[14] and emits electromagnetic waves. As the magnetization damping in $Y_3Fe_5O_{12}$ is very small[3], this cancellation is achieved by a small amount of STT. In contrast, when $J<0$ ($J>0$) at $\theta=90°$ ($\theta=-90°$), STT and the damping torque are parallel and cannot be cancelled out[22] (Fig. 3c).

We measured the power spectra $S(j)$, where j is electric current density, of microwaves emitted from the Pt/$Y_3Fe_5O_{12}$ film using an antenna while applying an electric current to the Pt layer. In Fig. 3d, we show $\Delta S(j)\equiv S(j)-S(-j)$ spectra at various values of j when $H=1.2$ kOe ($>H_C$). When the applied magnetic field is in the direction along the electric current, $\theta=0$, there are no emission signals in $\Delta S(j)$. In contrast, when the field is perpendicular to the current, $\theta=90°$, multiple peak signals appear in the spectra when j is greater than 4.4×10^8 A m^{-2} ($\equiv j_c$), as shown in Fig. 3d. The peak frequencies in the spectra vary with the magnetic field (Fig. 3f and i). The solid curve in Fig. 3i represents the ferromagnetic resonance frequencies calculated from the Kittel equation (see Supplementary Information section C for details); these peaks evidently originate from the spontaneous magnetization oscillations induced when $j>j_c$. The multiple peaks (see Fig. 3d) may be attributed to magnetostatic spin-wave modes which are excited simultaneously in the $Y_3Fe_5O_{12}$ layer (see Supplementary Information section D for details), but the strong change in the whole spectral shape with current and field strengths suggests the appearance of chaos[25] or the spin-diffusion-induced instability[26] in magnetization dynamics. In the j dependence of the frequency-integrated intensities for the $\Delta S(j)$ spectra, a clear threshold is observed at j_c (Fig. 3g). This implies that STT compensates the magnetization damping torque at $j=j_c$. The centroid frequency of the emission spectra decreases slightly with the current, a tendency which follows that in current-injection-type magnetization oscillations[27,28]. We checked that these peak signals disappear both in Pt/$Gd_3Ga_5O_{12}$ and Cu/$Y_3Fe_5O_{12}$ (Fig. 3e and h) films.

Finally, we show electric-signal transmission in the insulator $Y_3Fe_5O_{12}$ film by making use of these phenomena together. Figure 4a is a schematic illustration of the experimental set-up. Two Pt films (i and o) are sputtered on a single-crystal $Y_3Fe_5O_{12}$ film and an electric current is applied to the Pt film i. The distance between the films i and o is 1 mm, shorter than the spin-wave decay length in $Y_3Fe_5O_{12}$ crystals[3]. In this set-up, the electric current applied to the Pt film i induces magnetization oscillation in the $Y_3Fe_5O_{12}$ layer due to the STT across the Pt/$Y_3Fe_5O_{12}$ interface, as demonstrated in Fig. 3. This magnetization oscillation then propagates in the $Y_3Fe_5O_{12}$ layer via a spin-wave spin current. Figure 4b shows a numerical calculation of this propagation. When the oscillation reaches the second interface, it generates electric voltage in the Pt film o via spin pumping and ISHE, as demonstrated in Fig. 2. As shown in Figs 1c and 3b, these effects are activated when $j>0$ ($j<0$) at $\theta=90°$ ($\theta=-90°$)[9,22]. We measured the voltage generated in the Pt film o while applying electric currents to the Pt film i.

Figures 4c and d show the voltage difference V between the ends of the Pt film o as a function of the electric current density j in the Pt film i. When the magnetization of the $Y_3Fe_5O_{12}$ layer is along the electric current, $\theta=0$ and 180°, no signal appears in V (Fig. 4c). At $\theta=0$ and 180°, the above spin-transfer and voltage-generation mechanisms are inactive, and this result also confirms that the two Pt films are well isolated electrically. When $\theta=90°$ ($\theta=-90°$), in contrast, the voltage V signal appears with application of a current $j>6.0\times10^8$ A m^{-2} ($j<-6.0\times10^8$ A m^{-2}), as shown in Fig. 4d. We found that there is a clear threshold at 6.0×10^8 A m^{-2} in the j dependence of V (Fig. 4d). This threshold current density is comparable to that for the current-induced magnetization oscillation shown in Fig. 3g. All these results are consistent with the prediction that electric-signal transmission in the $Y_3Fe_5O_{12}$ is activated when $j>|j_c|$ ($j<-|j_c|$) at $\theta=90°$ ($\theta=-90°$), where $|j_c|$ is a threshold current density. If the distance between the Pt films were less than

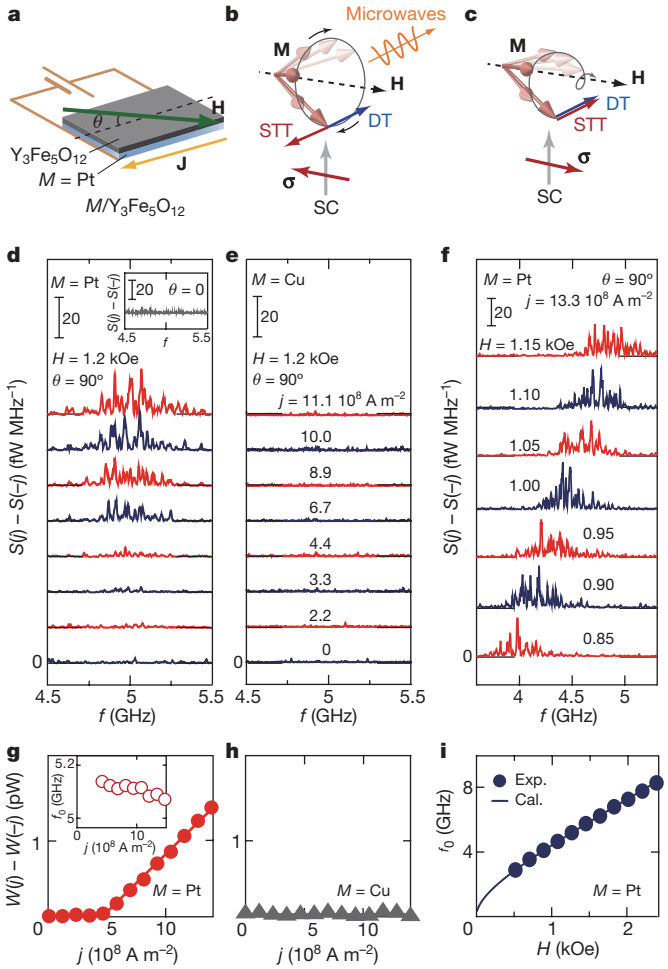

Figure 3 | Magnetization oscillation induced by spin-transfer torque in Pt/$Y_3Fe_5O_{12}$. **a**, Schematic illustration of the experimental set-up; the sample film is that shown in Fig. 2a. θ denotes the angle between the external in-plane magnetic field **H** and the direction along the electric current **J** in the Pt layer. **b**, **c**, Schematic illustrations of the directions of spin-transfer torque (STT) acting on the magnetization (**M**) and the magnetization-damping torque (DT) of the $Y_3Fe_5O_{12}$ layer at $\theta=90°$ when $J>0$ (**b**) and $J<0$ (**c**). J, amplitude of **J**; **σ**, spin polarization of the spin current (SC) induced from **J** by the spin-Hall effect in the Pt layer. **d**, **e**, $\Delta S(j)\equiv S(j)-S(-j)$ spectra for various values of the current density j in the Pt layer at $\theta=90°$ for Pt/$Y_3Fe_5O_{12}$ (**d**) and Cu/$Y_3Fe_5O_{12}$ (**e**) films when $H=1.2$ kOe. $S(j)$, the frequency f power spectrum of the microwaves (see Methods). In $\Delta S(j)$, background noise is eliminated as the antisymmetric component with respect to j is extracted. Inset to **d**, $\Delta S(j)$ spectrum at $\theta=0$ for the Pt/$Y_3Fe_5O_{12}$ film measured with application of $j=11.1\times10^8$ A m^{-2} when $H=1.2$ kOe. **f**, $\Delta S(j)$ spectra for various magnetic field strengths H for the Pt/$Y_3Fe_5O_{12}$ film measured when $j=13.3\times10^8$ A m^{-2} at $\theta=90°$. **g**, **h**, Values of the frequency integral from 4.5 GHz up to 5.5 GHz of the $\Delta S(j)$ spectra for the Pt/$Y_3Fe_5O_{12}$ film (shown in **d**), and for the Cu/$Y_3Fe_5O_{12}$ film (shown in **e**), respectively, as functions of j. **i**, H dependence of the centroid frequencies f_0 of the $\Delta S(j)$ spectra shown in **f**.

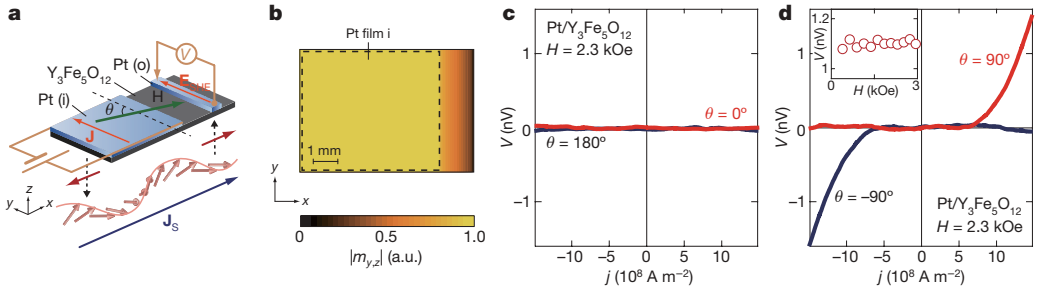

Figure 4 | Electric-signal transmission via spin-wave spin currents. a, A schematic illustration of the experimental set-up. The sample is a 1.3-μm-thick single-crystal $Y_3Fe_5O_{12}$ (111) film on which two separate 15-nm-thick Pt films (i and o) are sputtered. The distance between the Pt films is 1 mm. The surfaces of the $Y_3Fe_5O_{12}$ layer, Pt film i and Pt film o are rectangular shapes of area (mm^2) 35, 27.5 and 0.5, respectively. The distance between the voltage electrodes (V) attached to the Pt film o is 5 mm. **b**, In-plane spatial distribution of the time average of the magnetization-precession amplitude $|m_{y,z}|$ in the $Y_3Fe_5O_{12}$ layer numerically calculated using a stochastic Landau–Lifshitz–Gilbert equation[30] at room temperature. In the calculation, STT[22] that compensates the magnetization-damping torque at the Pt film i/$Y_3Fe_5O_{12}$ interface (dashed rectangle) is taken into consideration. Time average is taken for 1 μs (Supplementary Information section F). **c**, **d**, V as a function of j in the Pt film i at $\theta = 0^\circ$ (red curve in **c**), $\theta = 180^\circ$ (blue curve in **c**), $\theta = 90^\circ$ (red curve in **d**) and $\theta = -90^\circ$(blue curve in **d**). θ is defined in **a**. An in-plane magnetic field of 2.3 kOe is applied. Inset to **d**, V at $j = 16.6 \times 10^8$ A m^{-2} as a function of H (0.2 kOe $< H <$ 3 kOe) when $\theta = 90^\circ$.

nanometres, electron tunnelling could convey spin angular momentum; in the present macroscopic-sized system, in contrast, the tunnelling is clearly irrelevant. We confirmed that the electric-signal transmission disappears again both in Pt/$Gd_3Ga_5O_{12}$/Pt and Cu/$Y_3Fe_5O_{12}$/Cu systems. The results also indicate that the electric polarization in the insulator is irrelevant. The inset to Fig. 4d shows V at $j = 16.6 \times 10^8$ A m^{-2} as a function of magnetic field strength H (0.2 kOe $< H <$ 3 kOe) when $\theta = 90^\circ$. In this field range, V is minimally affected by the field-strength change and the role of the field seems to be no more than that of aligning the magnetization direction. This j dependence of V at $\theta = 90^\circ$ above $j = 6.0 \times 10^8$ A m^{-2} deviates from the linear dependence observed in Fig. 3g. This might be because not all the modes contribute equally to this transmission and the population of each mode may depend on the excitation strength (because of the intermode coupling or the spin-wave nonlinearity), but this discrepancy needs to be quantitatively elucidated.

The observed voltage transmission in an insulator provides a new method of signal transfer, and opens the door to insulator-based spintronics. The observed magnetization oscillation induced by the spin-Hall effect could also be applied to the construction of a microwave generator. We note that spin pumping from the insulator enables spin injection free from the conventional impedance-matching condition[12]. Finally, we anticipate that use of this spin transfer in insulators will lead to substantial advances in spintronics and electronics.

METHODS SUMMARY

A single-crystal $Y_3Fe_5O_{12}$ (111) film was grown on a $Gd_3Ga_5O_{12}$ (111) single-crystal substrate by liquid phase epitaxy. For the film growth, we used PbO-B_2O_3 flux around 1,200 K. Then, a 10-nm-thick Pt layer was sputtered on the $Y_3Fe_5O_{12}$ layer. Immediately before the sputtering, the surface was cleaned through the metal mask by Ar-ion bombardment in a vacuum. For the spin pumping measurements shown in Fig. 2, the Pt/$Y_3Fe_5O_{12}$ sample system was placed near the centre of a TE_{011} microwave cavity; at this position, the magnetic-field component of the microwave mode is maximized while the electric-field component is minimized. The microwave power was less than 10 mW, a value lower than the saturation of the ferromagnetic resonance absorption for the present sample. For measuring voltage induced by the spin pumping, a twisted pair of thin coated Cu wires (0.08 mm in diameter) are connected to the ends of the Pt layer. Microwave emission spectra were measured by attaching a gold coplanar-waveguide antenna to the Pt surface of the Pt/$Y_3Fe_5O_{12}$ sample film. The microwave signal received by the antenna was led to an amplifier via a microwave probe. The amplified microwave signal was analysed and recorded by a spectrum analyser. Micromagnetic simulation was performed by solving numerically the Landau–Lifshitz–Gilbert equation in which the spin torque at the interface cells are taken into consideration (for details, see Methods).

Full Methods and any associated references are available in the online version of the paper at www.nature.com/nature.

Received 28 September 2009; accepted 1 February 2010.

1. Ashcroft, N. W. & Mermin, N. D. *Solid State Physics* Ch. 9 (Saunders College, 1976).
2. Maekawa, S. (ed.) *Concepts in Spin Electronics* Ch. 7 and 8 (Oxford Univ. Press, 2006).
3. Schneider, T. *et al.* Realization of spin-wave logic gates. *Appl. Phys. Lett.* **92,** 022505 (2008).
4. Dyakonov, M. I. & Perel, V. I. Current-induced spin orientation of electrons in semiconductors. *Phys. Lett. A* **35,** 459–460 (1971).
5. Hirsch, J. E. Spin Hall effect. *Phys. Rev. Lett.* **83,** 1834–1837 (1999).
6. Takahashi, S. & Maekawa, S. Hall effect induced by a spin-polarized current in superconductors. *Phys. Rev. Lett.* **88,** 116601 (2002).
7. Kato, Y. K., Myers, R. C., Gossard, A. C. & Awschalom, D. D. Observation of the spin Hall effect in semiconductors. *Science* **306,** 1910–1913 (2004).
8. Wunderlich, J., Kaestner, B., Sinova, J. & Jungwirth, T. Experimental observation of the spin-Hall effect in a two-dimensional spin-orbit coupled semiconductor system. *Phys. Rev. Lett.* **94,** 047204 (2005).
9. Saitoh, E., Ueda, M., Miyajima, H. & Tatara, G. Conversion of spin current into charge current at room temperature: inverse spin-Hall effect. *Appl. Phys. Lett.* **88,** 182509 (2006).
10. Valenzuela, S. O. & Tinkham, M. Direct electronic measurement of the spin Hall effect. *Nature* **442,** 176–179 (2006).
11. Kimura, T., Otani, Y., Sato, T., Takahashi, S. & Maekawa, S. Room-temperature reversible spin Hall effect. *Phys. Rev. Lett.* **98,** 156601 (2007).
12. Valet, T. & Fert, A. Theory of the perpendicular magnetoresistance in magnetic multilayers. *Phys. Rev. B* **48,** 7099–7113 (1993).
13. Takahashi, S. & Maekawa, S. Spin current in metals and superconductors. *J. Phys. Soc. Jpn* **77,** 031009 (2008).
14. Kittel, C. *Introduction to Solid State Physics* 8th edn, Ch. 12 and 13 (Wiley, 2005).
15. Demokritov, S. O., Hillebrands, B. & Slavin, A. N. Brillouin light scattering studies of confined spin waves: linear and nonlinear confinement. *Phys. Rep.* **348,** 441–489 (2001).
16. Bass, J. & Pratt, W. P. Jr. Spin-diffusion lengths in metals and alloys, and spin-flipping at metal/metal interfaces: an experimentalist's critical review. *J. Phys. Condens. Matter* **19,** 183201 (2007).
17. Silsbee, R. H., Janossy, A. & Monod, P. Coupling between ferromagnetic and conduction-spin-resonance modes at a ferromagnetic-normal-metal interface. *Phys. Rev. B* **19,** 4382–4399 (1979).
18. Tserkovnyak, Y., Brataas, A. & Bauer, G. E. W. Enhanced Gilbert damping in thin ferromagnetic films. *Phys. Rev. Lett.* **88,** 117601 (2002).
19. Mizukami, S., Ando, Y. & Miyazaki, T. Effect of spin diffusion on Gilbert damping for a very thin permalloy layer in Cu/permalloy/Cu/Pt films. *Phys. Rev. B* **66,** 104413 (2002).
20. Kiselev, S. I. *et al.* Microwave oscillations of a nanomagnet driven by a spin-polarized current. *Nature* **425,** 380–383 (2003).
21. Ji, Y., Chien, C. L. & Stiles, M. D. Current-induced spin-wave excitations in a single ferromagnetic layer. *Phys. Rev. Lett.* **90,** 106601 (2003).
22. Ando, K. *et al.* Electric manipulation of spin relaxation using the spin Hall effect. *Phys. Rev. Lett.* **101,** 036601 (2008).
23. Brataas, A., Bauer, G. E. W. & Kelly, P. J. Non-collinear magnetoelectronics. *Phys. Rep.* **427,** 157–255 (2006).
24. Chikazumi, S. *Physics of Ferromagnetism* Ch. 20 and 21 (Oxford Univ. Press, 1997).

25. Stiles, M. D., Xiao, J. & Zangwill, A. Phenomenological theory of current-induced magnetization precession. *Phys. Rev. B* **69,** 054408 (2004).
26. Wigen, P. E., Doetsch, H., Ming, Y., Baselgia, L. & Waldner, F. Chaos in magnetic garnet thin films. *J. Appl. Phys.* **63,** 4157–4159 (1988).
27. Rippard, W. H., Pufall, M. R., Kaka, S., Russek, S. E. & Silva, T. J. Direct-current induced dynamics in $Co_{90}Fe_{10}/Ni_{80}Fe_{20}$ point contacts. *Phys. Rev. Lett.* **92,** 027201 (2004).
28. Krivorotov, I. N. *et al.* Large-amplitude coherent spin waves excited by spin-polarized current in nanoscale spin valves. *Phys. Rev. B* **76,** 024418 (2007).
29. Laulicht, I., Suss, J. T. & Barak, J. The temperature dependence of the ferromagnetic and paramagnetic resonance spectra in thin yttrium-iron-garnet films. *J. Appl. Phys.* **70,** 2251–2258 (1991).
30. Brown, W. F. Jr. Thermal fluctuations of a single-domain particle. *Phys. Rev.* **130,** 1677–1686 (1963).

Supplementary Information is linked to the online version of the paper at www.nature.com/nature.

Acknowledgements We thank K. Sato, Y. Suzuki, Y. Tserkovnyak, G. Tatara, T. Ishibashi and K. M. Itoh for discussions. This work was supported by a Grant-in-Aid for Scientific Research in Priority Area 'Creation and control of spin current' (19048028) from MEXT, Japan, a Grant-in-Aid for Scientific Research (A) from MEXT, Japan, the global COE for the 'Materials integration international centre of education and research' and 'High-level global cooperation for leading-edge platform on access spaces (C12)' from MEXT, Japan, a Grant for Industrial Technology Research from NEDO, Japan, and Fundamental Research Grant from TRF, Japan.

Author Contributions Y.K., K.H., K.U. and K.A. performed the measurements and analysed the data; J.O. carried out the numerical analysis; S.T., S.M. and E.S. provided the theoretical analysis; H.U. and H.K. contributed to the sample fabrication; Y.K., K.H, K.U., M.M. and K.T. contributed to the experimental set-up; Y.K., S.T., J.O., K.U., M.M., H.U., K.T., S.M. and E.S. wrote the manuscript; all authors discussed the results and commented on the manuscript; and E.S. planned and supervised the project.

Author Information Reprints and permissions information is available at www.nature.com/reprints. The authors declare no competing financial interests. Correspondence and requests for materials should be addressed to E.S. (saitoheiji@imr.tohoku.ac.jp).

METHODS

Film preparation. A single-crystal $Y_3Fe_5O_{12}$ (111) film was grown on a 0.5-mm-thick $Gd_3Ga_5O_{12}$ (111) single-crystal substrate by liquid phase epitaxy. For the film growth, we used PbO-B_2O_3 flux around 1,200 K. Then, a 10-nm-thick Pt layer was sputtered on the $Y_3Fe_5O_{12}$ layer through a metal mask using a sputtering and etching system (K-Science KE604TT1-S2B). Immediately before the sputtering, the surface was cleaned through the metal mask by Ar-ion bombardment in a vacuum. The chemical composition and crystalline structure of the film were confirmed by X-ray fluorescence spectroscopy and X-ray diffractometry, respectively. The magnetization-saturation field for the $Y_3Fe_5O_{12}$ layer was estimated by measuring the magnetic-field dependence of a magneto-optical Kerr effect signal induced by He-Ne laser light (632.8 nm) in a cross-Nicol configuration.

Spin pumping measurements shown in Fig. 2. The Pt/$Y_3Fe_5O_{12}$ sample system was placed near the centre of a TE_{011} microwave cavity at which the magnetic-field component of the microwave mode is maximized while the electric-field component is minimized. During the measurements, the microwave mode with a frequency of 9.44 GHz was exited in the cavity, and an external static magnetic field **H** was applied along the film. The microwave power was less than 10 mW, a value lower than the saturation of the ferromagnetic resonance absorption for the present sample. The microwave absorption was detected using a spectrometer (JEOL JES-FA200) connected to the cavity. For voltage measurements, two 100-nm-thick 0.5-mm-wide Pt electrodes were sputtered on the ends of the Pt film. A twisted pair of thin coated Cu wires (0.08 mm in diameter) is connected to the electrodes with silver paste. The voltage difference between these two wires was measured using a lock-in amplifier (NF LI5640) and a volt meter (Keithley 2000) via an amplifier (DL-instruments 1201).

Microwave emission measurements shown in Fig. 3. A gold coplanar-waveguide antenna, whose centre-conductor width is 100 μm, was attached to the Pt surface of the Pt/$Y_3Fe_5O_{12}$ sample film. The microwave signal received by the antenna was led to an amplifier (Miteq AFS44-00102000-30-10P-44) via a microwave probe (Picoprobe 40A-GSG-100-VP-NM). The amplified microwave signal was analysed and recorded by a spectrum analyser (Anritsu MS2687B).

Non-local *I*–*V* measurements shown in Fig. 4. The sample film was fixed on a sample stage of a micro-prober system (Nagase GRAIL-103054LVMG) and electric connections were made with the microprobes. An electric current was applied to the Pt film i with a voltage-function generator (NF WF1946B) and a hand-made current amplifier. The voltage signal in the Pt film o was led to a storage scope (Tektronix TDS1001) and to a lock-in amplifier (NF LI5640) via a preamplifier (DL-instruments 1201). Precise *I*–*V* measurements were performed with the lock-in amplifier by modulating sinusoidally the input d.c. current and then by integrating the lock-in signal with respect to the current. Before the precise measurement, we performed rough measurements to see the overall behaviour of *V*; we measured d.c. voltage *V* using the storage scope with changing input current without sinusoidal modulations.

Micromagnetic simulation. We numerically solved the Landau–Lifshitz–Gilbert equation:

$$\frac{d\mathbf{M}}{dt} = -\gamma(\mathbf{H}_{eff} \times \mathbf{M}) + \frac{\alpha}{M_s}\mathbf{M} \times \frac{d\mathbf{M}}{dt} + \boldsymbol{\tau}_{stt}$$

by using the object-oriented micromagnetic framework[31] extended to the fourth order Runge-Kutta method. Here, $\gamma = 1.76 \times 10^7\ \mathrm{Oe}^{-1}\,\mathrm{s}^{-1}$ is the gyromagnetic ratio, $4\pi M_s = 1{,}956$ Oe is the saturation magnetization and $\alpha = 6.7 \times 10^{-5}$ is the Gilbert damping coefficient. The field $\mathbf{H}_{eff}$ is an effective magnetic field which includes an applied magnetic field $\mathbf{H}_{dc} = 2.3$ kOe, an exchange field $\mathbf{H}_{ex} = (2A/M_s^2)\nabla^2\mathbf{M}$ due to the ferromagnetic coupling where the exchange stiffness $A = 4.73 \times 10^{-12}\ \mathrm{J\,m}^{-1}$, the demagnetization field $\mathbf{H}_{demag}$ and the random magnetic field due to the thermal effect[30]. $\boldsymbol{\tau}_{stt} = c\mathbf{M} \times (\mathbf{s} \times \mathbf{M})$ represents the spin torque term due to the transmission of angular momentum from Pt film i to $Y_3Fe_5O_{12}$ via an exchange interaction (see Supplementary Information section B for details). When the static field $\mathbf{H}_{dc}$ is applied, the spin torque term $\boldsymbol{\tau}_{stt}$ points to the direction opposite to the damping vector $\mathbf{M} \times d\mathbf{M}/dt$. For realizing the experimental condition where the input is the threshold current, the parameter *c* was chosen so that the magnitude is that of the damping term. We calculated the time average of the out-of-plane component of the magnetization. The gradation of the colour indicates that the spin-wave spin current propagates in the *x* direction.

31. Donahue, M. J. & Porter, D. G. OOMMF v1.2a3 Object Oriented MicroMagnetic Framework Software (NIST, 2004).

A. Spin current and spin-wave spin current

Conduction electrons in metallic conductors carry charge and spin. In a ferromagnetic metal (F), both charge and spin currents flow by application of bias voltage, since the spins of conduction electrons are spontaneously polarized. In a nonmagnetic metal (N), spin current is created by spin injection from a ferromagnet attached to N or by the spin Hall effect in N, in which up-spin and down-spin electrons flow in the opposite directions without charge current, resulting in the so-called "pure spin current". In this way, the spin current is able to flow in metallic conductors[2].

Ferromagnetic insulators, on the other hand, have different properties that they are electrically inactive with frozen charge degrees of freedom, but magnetically active due to the spins of localized electrons. The low-lying magnetic excitations are spin waves whose propagation carries spin angular momentum.

The low-lying magnetic excitation of spin waves is described by the Landau-Lifshitz-Gilbert equation[32]

$$\frac{\partial}{\partial t}\mathbf{M}(\mathbf{r},t) = \gamma \mathbf{H}_{\mathrm{i}} \times \mathbf{M}(\mathbf{r},t) - \frac{D}{\hbar M_s}\mathbf{M} \times \nabla^2 \mathbf{M}(\mathbf{r},t) + \frac{\alpha}{M_s}\mathbf{M}(\mathbf{r},t) \times \frac{\partial}{\partial t}\mathbf{M}(\mathbf{r},t) \qquad \text{(S1)}$$

where γ is the gyromagnetic ratio, $\mathbf{H}_{\mathrm{i}} = (0,0,H_{\mathrm{i}})$ is an internal field along the **z** direction, D is the exchange stiffness, α is the Gilbert damping constant. Equation (S1) has solutions $M_+(\mathbf{r},t) = M_x(\mathbf{r},t) + iM_y(\mathbf{r},t) \propto \exp(i\mathbf{q}\cdot\mathbf{r} + i\omega_q t)\exp(-\alpha\omega_q t)$ with the spin wave dispersion

$\hbar\omega_q = \hbar\gamma H_{\rm i} + Dq^2$ and the damping $\alpha\omega_q$. In the following, the Gilbert damping term is disregarded for simplicity. Then, equation (S1) is rewritten as

$$\frac{\partial}{\partial t}\mathbf{M}(\mathbf{r},t) = \gamma\mathbf{H}_{\rm i}\times\mathbf{M}(\mathbf{r},t) - \nabla\cdot\mathbf{J}^{\mathbf{M}}(\mathbf{r},t) \qquad \text{(S2)}$$

where $\mathbf{J}^{\mathbf{M}}$ is the magnetization current, which we call the *spin-wave spin current*, whose components are

$$J_j^{M_\alpha} = \frac{D}{\hbar M_s}[\mathbf{M}\times\nabla_j\mathbf{M}]_\alpha = \frac{D}{\hbar M_s}\varepsilon_{\alpha\mu\nu}\mathbf{M}_\mu\nabla_j\mathbf{M}_\nu \qquad \text{(S3)}$$

Here, label α is the α-th component of the magnetization vector, label j is the j-th component of the flow direction, $\varepsilon_{\alpha\mu\nu}$ is Levi-Civita antisymmetric symbol. Note that the z-component of equation (S2) gives the conservation $\partial_t M_z + \nabla\cdot\mathbf{J}^{M_z} = 0$ in case of $\alpha = 0$.

By introducing $\psi(\mathbf{r},t) = M_+(\mathbf{r},t) = M_x(\mathbf{r},t) + iM_y(\mathbf{r},t)$ and its conjugate complex $\psi^*(\mathbf{r},t)$, the z-component of the spin-wave spin current is written as

$$\mathbf{J}^{M_z} = \frac{1}{2i}\frac{D}{\hbar M_s}\left[\psi^*(\mathbf{r},t)\nabla\psi(\mathbf{r},t) - \psi(\mathbf{r},t)\nabla\psi^*(\mathbf{r},t)\right] \qquad \text{(S4)}$$

Using the creation and annihilation operators $(b_q^\dagger, b_q)$ of spin-wave excitations with energy ω_q and momentum q by the transformations, $\psi = M_+ = \sqrt{2\hbar\gamma M_s}\sum_q b_q e^{i\mathbf{q}\cdot\mathbf{r}}$ and $\psi^* = M_- = \times\sqrt{2\hbar\gamma M_s}\sum_q b_q^\dagger e^{-i\mathbf{q}\cdot\mathbf{r}}$, the spin-wave spin current is expressed in the second-quantized form, whose expectation value is

$$\mathbf{J}^{M_z} = \hbar\gamma\sum_q \mathbf{v}_q n_q \qquad \text{(S5)}$$

where $\mathbf{v}_q = \partial\omega_q/\partial\mathbf{q} = 2(D/\hbar)\mathbf{q}$ is the spin-wave velocity and $n_q = \langle b_q^\dagger b_q\rangle$ is the distribution function of spin-waves. Equation (S5) indicates that, when the population of spin waves is different between $\mathbf{q}$ and $-\mathbf{q}$ in the wave-vector space, the spin waves carry the spin-wave spin

current.

In metals, on the other hand, the spin current is carried by conduction electrons, and is expressed by

$$\mathbf{J}^{m_z} = \frac{1}{2}\hbar\gamma_e \sum_k \mathbf{v}_k (f_{k\uparrow} - f_{k\downarrow}) \tag{S6}$$

where γ_e is the gyromagnetic ratio, $\mathbf{v}_k$ is the velocity, and $f_{k\sigma}$ is the distribution function of conduction electrons with spin σ and momentum k. In the spin transport of drift-diffusion, $\mathbf{j}^{m_z} = -D_{\mathrm{N}} \nabla \delta m_{\mathrm{N}}^z$, where D_{N} is the diffusion constant and δm_{N}^z is the magnetization due to spin accumulation in N.

We next consider a junction which consists of a ferromagnetic insulator (FI) and normal metal (N), and investigate how the spin current flows through the interface of the junction, when spins are accumulated in the N layer. The spin accumulation is represented by the splitting $\delta\mu = \mu_\uparrow - \mu_\downarrow$ of the up-spin and down-spin chemical potential. The magnetizations of FI and N are assumed to be oriented in the z direction. In this situation, the exchange interaction between spins of conduction electrons and localized spins at the interface play a crucial role for the flow of spin current through the interface.

When conduction electrons in N are incident on FI, the electrons are reflected back at the FI/N interface, since electrons are prohibited to enter FI due to the large energy gap at the Fermi energy. At the scattering, there are quantum-mechanical spin-flip processes due to the spin-exchange interaction, in which an electron reverses its spin, thereby emitting or absorbing a spin wave in FI. The spin-flip scattering with spin-wave excitation gives rise to

transfer of spin angular momentum between FI and N. When the up-spin chemical potential is higher than the down-spin chemical potential, the spin-flip process from up-spin to down-spin state dominates over the reversed process, so that the spin current flows from N to FI across the FI/N interface[33].

We describe the exchange interaction between local moments and conduction electrons at the interface by the *s*-*d* exchange interaction,

$$H_{\rm sd} = \frac{J_{\rm sd}}{N_e}\sum_{n=1}^{N_{\rm I}} \boldsymbol{S}_n \cdot \psi^{\dagger}_{\sigma'}(\boldsymbol{r}_n)\hat{\boldsymbol{\sigma}}_{\sigma'\sigma}\psi_{\sigma}(\boldsymbol{r}_n) \qquad \text{(S7)}$$

where $\mathbf{S}_n$ are local moments at position $\mathbf{r}_n$ on the interface, $\psi^{\dagger}_{\sigma}(\boldsymbol{r}_n)$ and $\psi_{\sigma}(\boldsymbol{r}_n)$ are the creation and annihilation operators of an incident electron with spin σ at position $\mathbf{r}_n$, respectively, $\hat{\boldsymbol{\sigma}}$ is the Pauli spin operator, N_e is the number of electrons in the N layer and, $N_{\rm I}$ is the number of local moments that interact with conduction electrons at the interface. Making use of the Fourier transformation $\psi_{\sigma}(\mathbf{r}) = \sum_{\mathbf{k}} c_{k\sigma} e^{i\mathbf{k}\cdot\mathbf{r}}$ and $S_n^{\pm} = S_n^x \pm iS_n^y = N_S^{-1/2}\sum_{\mathbf{q}} S_q^{\pm} e^{i\mathbf{q}\cdot\mathbf{r}}$, where N_S is the number of localized spins in the FI layer, equation (S1) can be written in the momentum representation.

Using the Heisenberg equation of motion, the spin current $J^{m_z} = \mu_{\rm B}(d/dt)(N_e^{\uparrow} - N_e^{\downarrow})$ (N_e^{σ} is the number of conduction electrons with spin σ) is expressed as

$$J^{m_z} = i\gamma_e J_{\rm eff}\sum_{\mathbf{k},\mathbf{p},\mathbf{q}} e^{i\delta\mu t/\hbar} S^{-}_{-\mathbf{q}}(t) c^{\dagger}_{\mathbf{k}\uparrow}(t) c_{\mathbf{p}\downarrow}(t)\rho^{*}_{\mathbf{q}-\mathbf{p}+\mathbf{k}} - i\gamma_e J_{\rm eff}\sum_{\mathbf{k}',\mathbf{p}} e^{-i\delta\mu t/\hbar} S^{+}_{\mathbf{q}}(t) c^{\dagger}_{\mathbf{p}\downarrow}(t) c_{\mathbf{k}\uparrow}(t)\rho_{\mathbf{q}-\mathbf{p}+\mathbf{k}} \qquad \text{(S8)}$$

where $J_{\rm eff} = J_{\rm sd}/(N_e N_S^{1/2})$, $c^{\dagger}_{\mathbf{k}\sigma}(c_{\mathbf{k}\sigma})$ is the creation (annihilation) operator of an electron with momentum $\mathbf{k}$ and spin σ, and $\rho_{\mathbf{q}-\mathbf{p}+\mathbf{k}} = \sum_{n=1}^{N_{\rm I}} e^{i(\mathbf{q}-\mathbf{p}+\mathbf{k})\cdot\mathbf{r}_n}$.

The spin current across the interface is calculated by the linear-response theory

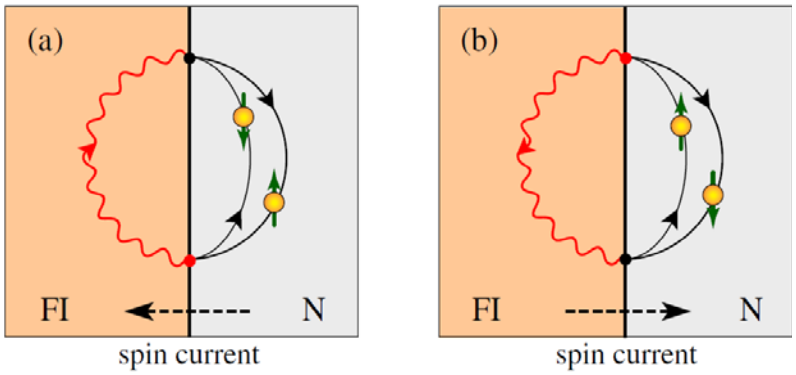

Figure S1: Feynman diagrams for the spin current through the FI/N interface in the left direction (a) and the right direction (b). The wavy lines in FI represent the spin-wave propagators and the solid lines in N the electron propagators. Spin waves are emitted or absorbed by spin-flip reflection of electrons at the interface, by which spin angular momentum is transferred between FI and N.

$$J^{m_z} = -\frac{i}{\hbar}\int_{-\infty}^{t} dt' \left\langle \left[\hat{J}^{m_z}(t), H_{sd}(t') \right] \right\rangle \tag{S9}$$

Figure S1 shows the Feynman diagrams for the spin current flowing in the left and right directions across the interface. At the interface, spin waves are emitted or absorbed by spin-flip reflection of electrons at the interface. Using the Green's function methods, we have the spin current across the interface[33]

$$J^{m_z} = 4\pi\gamma_e N_I \langle S_z \rangle [J_{sd} v_e N(0)]^2 N_S^{-1} \sum_{\mathbf{q}} (\hbar\omega_q + \delta\mu) \left[\frac{1}{e^{(\hbar\omega_q + \delta\mu)/k_B T} - 1} - \frac{1}{e^{\hbar\omega_q / k_B T} - 1} \right] \tag{S10}$$

where $N(0)$ is the density of states of conduction electrons at the Fermi level and v_e is the volume per electron. Equation (S10) indicates that the spin accumulation $\delta\mu$ plays a role of spin voltage which generates the spin current across the interface. Therefore, the spin current carried by conduction electrons given in equation (S6) is converted to the current carried by spin waves in equation (S5) through the interface spin current given in equation (S10).

B. Interface spin exchange coupling in $Pt/Y_3Fe_5O_{12}$

We show that the spin pumping in $Pt/Y_3Fe_5O_{12}$ originates from the spin exchange interaction between a conduction electron in Pt and a localized moment in $Y_3Fe_5O_{12}$ at the interface. We take into account the exchange interaction in the Landau-Lifshitz-Gilbert equation for the magnetization of $Y_3Fe_5O_{12}$ and the Bloch equation with spin diffusion for spin accumulation in Pt[17,18,34-36], and solve these coupled equations to calculate the spin current pumped from $Y_3Fe_5O_{12}$ into Pt. By combining the pumped spin current with the inverse spin-Hall effect (ISHE), we derive the output voltage V appeared between the Pt ends as a function of the exchange coupling.

At the interface of a normal metal (N) and a ferromagnetic insulator (FI), conduction electrons in N interact with magnetic moments of FI through the so-called *s*-*d* exchange interaction,

$$H_{\rm sd} = -J_{\rm sd} \sum_{i\in \rm I} \mathbf{S}_i \cdot \mathbf{s}_i \qquad \text{(S11)}$$

where $\mathbf{s}_i$ and $\mathbf{S}_i$ are the conduction-electron spin and the localized spin at site i on the interface, and $J_{\rm sd}$ is the exchange coupling strength between them. In the presence of microwave field, we assume a uniform precession of aligned localized spins, in which case $\mathbf{S}_i$ is replaced by the magnetization $\mathbf{M}$ using the relation $\mathbf{S}_i/S = \mathbf{M}/M_s$ [36], and rewrite equation (S11) as [17,18,34,35]

$$H_{\rm sd} = -J_{\rm ex} \int dx \mathbf{M}(t) a_{\rm eff} \delta(x) \cdot \mathbf{m}_{\rm N}(x,t) \qquad \text{(S12)}$$

where $J_{\rm ex} = J_{\rm sd} S/(\hbar \gamma_e M_s)$ is the dimensionless exchange coupling constant, S is an effective block spin per unit cell, γ_e is the gyromagnetic ratio of conduction electron, $a_{\rm eff} = v_e/a_S^2$ is the

effective interaction range, v_e is the volume per conduction electron, a_S is the lattice constant of localized spins at the interface, and $\mathbf{m}_{\mathrm{N}}(x,t)$ is the magnetization of conduction electrons. Equation (S12) indicates that $[\mathbf{M}(t)/M_s]a_{\mathrm{eff}}\delta(x)$ plays a role of the interface magnetization, which exerts the exchange spin torque on $\mathbf{m}_{\mathrm{N}}(x,t)$

$$\left[d\mathbf{m}_{\mathrm{N}}(x,t)/dt\right]_{\mathrm{exchange}} = -\gamma_e J_{\mathrm{ex}}\mathbf{m}_{\mathrm{N}}(x,t)\times\mathbf{M}(t)a_{\mathrm{eff}}\delta(x) \tag{S13}$$

through the exchange interaction at the interface. The magnetization of conduction electrons is written as $\mathbf{m}_{\mathrm{N}}(x,t) = \mathbf{m}_0 a_{\mathrm{eff}}\delta(x) + \delta\mathbf{m}_{\mathrm{N}}(x,t)$, where $\mathbf{m}_0 = \chi_{\mathrm{N}} J_{\mathrm{ex}}\mathbf{M}$ is the local equilibrium spin density, $\chi_{\mathrm{N}} = \mu_{\mathrm{B}}^2 N(0)$ is the spin susceptibility of conduction electrons, and $\delta\mathbf{m}_{\mathrm{N}}(x,t)$ is spin accumulation.

By taking into account the exchange spin torque as well as the spin diffusion, the Bloch equation for $\mathbf{m}_{\mathrm{N}}(x,t)$ is given by

$$\frac{\partial\mathbf{m}_{\mathrm{N}}(x,t)}{\partial t} = -\gamma_e J_{\mathrm{ex}}\left[\mathbf{m}_{\mathrm{N}}(x,t)\times\mathbf{M}(t)\right]a_{\mathrm{eff}}\delta(x) - \frac{\delta\mathbf{m}_{\mathrm{N}}(x,t)}{\tau_{\mathrm{sf}}} + D_{\mathrm{N}}\nabla^2\delta\mathbf{m}_{\mathrm{N}}(x,t) \tag{S14}$$

where τ_{sf} is the spin-flip relaxation time and D_{N} is the diffusion constant. By requiring that the precession frequency (~GHz) is much smaller than the spin-flip relaxation rate (τ_{sf}^{-1}~$10^{12}\mathrm{s}^{-1}$) and neglecting the small terms $M_{x(y)}\delta m_{\mathrm{N}}^z$, we obtain the solutions of equation (S14) for the transverse spin accumulation $\delta m_{\mathrm{N}}^{\pm}(x,t) = \delta m_{\mathrm{N}}^x(x,t) \pm i\delta m_{\mathrm{N}}^y(x,t)$, which are used to calculate the longitudinal spin accumulation $\delta m_{\mathrm{N}}^z(x) = (1/\Gamma)\,\mathrm{Im}\left[\delta m_{\mathrm{N}}^+(0,t)(M_-/M_z)\right]e^{-x/\lambda_{\mathrm{N}}}$ and the spin current $j_s^z = -(e/\mu_{\mathrm{B}})D_{\mathrm{N}}\nabla_x\delta m_{\mathrm{N}}^z$, which yields the pumped spin current

$$j_s^z(x) = -\frac{\hbar}{4e}\frac{\sigma_{\mathrm{N}}}{\lambda_{\mathrm{N}}}\frac{(\hat{\mathbf{M}}\times\partial_t\hat{\mathbf{M}})_z}{1+\Gamma^2}e^{-x/\lambda_{\mathrm{N}}} = \frac{\hbar\omega}{4e}\frac{\sigma_{\mathrm{N}}}{\lambda_{\mathrm{N}}}\frac{1}{1+\Gamma^2}\left(\frac{M_+M_-}{M_z^2}\right)e^{-x/\lambda_{\mathrm{N}}} \tag{S15}$$

where $\omega = 2\pi f$ (f is a microwave frequency), $M_{\pm}(t) = M_x(t) \pm iM_y(t)$, $\lambda_N = \sqrt{D_N \tau_{sf}}$ is the spin-diffusion length, $\Gamma = (\tau_{ex}/\tau_{sf})(\lambda_N/a_{eff})$ and $\tau_{ex} = \hbar/(SJ_{sd})$. Note that the factor (λ_N/a_{eff}) appears in Γ due to the exchange interaction restricted at the interface. Thus, the spin current strongly depends on the magnitude of the exchange coupling through Γ. For $\Gamma^2 << 1$, the spin current is independent of the exchange coupling. For $\Gamma^2 >> 1$, the spin current is proportional to the square of the exchange coupling. In in ordinary ferromagnets, $(\tau_{ex}/\tau_{sf}) << 1$, whereas $(\lambda_N/a_{eff}) >> 1$ due to the interface effect.

Using the solution of the Landau-Lifshitz-Gilbert equation for $\boldsymbol{M}$, we have

$$\left(\frac{M_+ M_-}{M_z^2}\right) = \frac{2\delta M_z}{M_z} = \frac{(\gamma h_{ac})^2}{(\omega - \gamma H)^2 + (\alpha\omega)^2} \qquad \text{(S16)}$$

where h_{ac} is the amplitude of microwave field, γ is the gyromagnetic ratio of FI, and α is the Gilbert damping constant which includes the additional damping α' due to spin pumping: $\alpha' = (m_0/M_s)(a_{eff}/d_F)\Gamma/(1+\Gamma^2) = [J_{sd} v_e N(0)](a_S/4d_F)\Gamma/(1+\Gamma^2)$ [37,38].

By taking into account the boundary condition that the spin current vanishes at the surface of N, $j_s^z(x = d_N) = 0$, we have the pumped spin current

$$j_s^N(x) = \frac{\hbar\omega}{4e}\frac{\sigma_N}{\lambda_N}\frac{\sinh[(d_N - x)/\lambda_N]}{\sinh(d_N/\lambda_N)}\frac{\tanh(d_N/\lambda_N)}{1+\Gamma^2\tanh^2(d_N/\lambda_N)}\left(\frac{M_+ M_-}{M_z^2}\right) \qquad \text{(S17)}$$

which gives rise to the electric field E along the y direction by the inverse spin-Hall effect (ISHE). Using $\sigma_N E = \alpha_{SHE}\langle j_s^N(x)\rangle$, where $\langle j_s^N(x)\rangle$ is the average of $j_s^N(x)$ over x, the induced voltage $V = \alpha_{SHE} w_N \rho_N \langle j_s^N(x)\rangle$ between the Pt ends with length w_N due to ISHE is given by

$$V \approx \alpha_{\mathrm{SHE}} \frac{\hbar\omega}{4e}\left(\frac{w_{\mathrm{N}}}{d_{\mathrm{N}}}\right)\frac{\tanh(d_{\mathrm{N}}/\lambda_{\mathrm{N}})\tanh(d_{\mathrm{N}}/2\lambda_{\mathrm{N}})}{1+\Gamma^2\tanh^2(d_{\mathrm{N}}/\lambda_{\mathrm{N}})}\left(\frac{M_+M_-}{M_z^2}\right) \quad \text{(S18)}$$

Equation (S18) enables us to estimate the magnitude of exchange interaction J_{sd} from a measured value of voltage V at resonance ($\omega = \gamma H$). Using the measured value $V = 4.8\mu\mathrm{V}$, together with experimental parameters: $d_{\mathrm{N}} = 10\mathrm{nm}$, $w_{\mathrm{N}} = 3\mathrm{mm}$, $\lambda_{\mathrm{N}} = 7\mathrm{nm}$, $\alpha_{\mathrm{SHE}} = 0.0037$, $\gamma = 1.76\times10^{7}\,\mathrm{Oe^{-1}s^{-1}}$, $\alpha = 6.7\times10^{-5}$, $f = 9.4\times10^{9}\,\mathrm{s^{-1}}$, $h_{ac} = 0.11\mathrm{Oe}$, we obtain the value of $\Gamma \approx 19$. From this Γ value and $\tau_{\mathrm{sf}} = 0.3\times10^{-12}\mathrm{s}$, $4\pi M_{\mathrm{s}} = 1{,}956$ Oe, $a_S \sim 1.24\mathrm{nm}$, and $S = M_s a_S^3/(\hbar\gamma) = 16$, the magnitude of the spin-exchange energy is estimated to be $J_{\mathrm{sd}} \sim 10$ meV, which is two orders of magnitude smaller than those of typical ferromagnets ($J_{\mathrm{sd}} \sim 1$ eV for Co, Fe, Ni and their alloys). The spin-exchange energy density at the interface is $SJ_{\mathrm{sd}}/a_S^2 \sim 16$ erg/cm^2.

The ISHE voltage in equation (S18) at resonance depends linearly on the microwave power. However, as the microwave power becomes large, one may expect that the pumped spin current will give rise to an additional backflow current due to the spin accumulation in N, which further modifies the Gilbert damping. If one writes the pumped spin current as $j_s = j_{s0}(\gamma h_{ac}/\tilde{\alpha}\omega)^2$ with $\tilde{\alpha} = \alpha + \beta(j_s/j_{s0})$ (β is a constant), one obtains the non-linear dependence of the microwave power as $j_s = 2\,j_{s0}(\gamma h_{ac}/\alpha\omega)^2/\left[1+\sqrt{1+8(\beta/\alpha)(\gamma h_{ac}/\alpha\omega)^2}\right]$. Therefore, the ISHE voltage $V(\propto j_s)$ behaves as $V \propto (\gamma h_{ac}/\alpha\omega)^2$ for a low microwave power while $V \propto (\gamma h_{ac}/\alpha\omega)$ for a high microwave power, which are in agreement with experimental observation in Fig. 2g.

According to the theory of spin-pumping based on the scattering formalism, we can also

estimate the spin mixing conductance $g_{\uparrow\downarrow}$ at the FI/N interface. Following the formalism in Refs. 23, 38 and 39, we obtain the pumped spin current into the N layer, which induces the voltage due to ISHE,

$$V = \alpha_{\mathrm{SHE}} \frac{\hbar\omega}{4e}\left(\frac{w_{\mathrm{N}}}{d_{\mathrm{N}}}\right)\frac{\frac{2e^2}{h}\frac{g_{\uparrow\downarrow}}{G_{\mathrm{N}}^{\mathrm{s}}}\tanh(d_{\mathrm{N}}/2\lambda_{\mathrm{N}})}{1+\frac{2e^2}{h}\frac{g_{\uparrow\downarrow}}{G_{\mathrm{N}}^{\mathrm{s}}}\coth(d_{\mathrm{N}}/\lambda_{\mathrm{N}})}\left(\frac{M_{+}M_{-}}{M_z^2}\right) \qquad \text{(S19)}$$

where $G_{\mathrm{N}}^{\mathrm{s}} = \sigma_{\mathrm{N}} A_{\mathrm{N}}/\lambda_{\mathrm{N}}$. By comparing equation (S19) with equation (S18), we find that the mixing conductance is related with the parameter Γ by $g_{\uparrow\downarrow} \approx (G_{\mathrm{N}}^{s}/\Gamma^2)(h/2e^2)$ in the case of Γ^2 >> 1, and obtain the mixing conductance $g_{\uparrow\downarrow}/A_{\mathrm{N}} \approx 3\times10^{12}\,\mathrm{cm}^{-2}$ at the interface of Pt/$Y_3Fe_5O_{12}$. We note that if the voltages in (S18) and (S19) are plotted as a function of Γ^{-2} and $(2e^2/h)g_{\uparrow\downarrow}/G_{\mathrm{N}}^{s}$, respectively, these curves have nearly the same values with each other.

C. Analysis of microwave emission frequencies

The variation of the centroid frequency of the emission spectra shown in Fig. 3i with changing the magnetic field is consistent with the Kittel equation for ferromagnetic resonance. The solid curve in Fig. 3i represents the ferromagnetic resonance frequencies calculated from the Kittel equation:

$$f = \frac{\gamma}{2\pi}\sqrt{(H + H_{\mathrm{an}} + H_{\mathrm{d}})(H + H_{\mathrm{an}} + H_{\mathrm{d}} + 4\pi M_{\mathrm{eff}})} \qquad \text{(S20)}$$

where $4\pi M_{\mathrm{eff}}$=1,956 Oe is the saturation magnetization of this $Y_3Fe_5O_{12}$ film. H_{an}, the effective anisotropy field, is the fitting parameter. The fitting result is H_{an}=8 Oe.

D. A hypothesis on the role of MSSW modes

Magnetostatic-surface-wave (MSSW) modes may be expected to be first excited by the spin torque since the modes are localized near the $Y_3Fe_5O_{12}$ surface and thus sensitive to the spin-transfer torque at the Pt/$Y_3Fe_5O_{12}$ interface. This excitation can be transferred into the other volume modes via the intermode coupling.

E. Experimental estimation of the Gilbert-damping coefficient for the $Y_3Fe_5O_{12}$ film

Figure 2b is the spectrum measured when a magnetic field is perpendicular to the film, a configuration where the resonance-field intervals among different SWR modes are enhanced. The arrows represent the fitting result for the spin-wave (exchange mode) resonance fields[29], from which the saturation magnetization $4\pi M_{\rm eff}$=1,956 Oe and the spin-exchange stiffness A=4.73×10^{-12} J/m for the present $Y_3Fe_5O_{12}$ film are obtained. N represents the spin-wave mode number along the direction perpendicular to the film. We estimated the spectral width for the N=1-mode via a fitting procedure using Lorentz-type dispersion functions. From the spectral width, we estimated the Gilbert-damping coefficient for the present $Y_3Fe_5O_{12}$ film to be 6.7×10^{-5}.

F. Micromagnetic simulation for the $Y_3Fe_5O_{12}$ layer

In order to calculate the spin dynamics excited by the spin pumping from the Pt-film **i**, we numerically solve the Landau-Lifshitz-Gilbert (LLG) equation (S1) by using the object-oriented micromagnetic framework (OOMMF)[31] extended to the 4th order Runge-Kutta method. We consider the demagnetization field $\mathbf{H}_{\rm demag}$ which is calculated by the

convolution of a kernel describing the dipole-dipole interaction between unit cells. The convolution is performed by using the fast Fourier transform technique. We also apply the random magnetic field due to the thermal effect[30]. We use parameters same as those in SI-B and the exchange stiffness A=4.73×10^{-12} J/m.

To confirm that the calculated model can describe the spin wave in the thin film, we first perform a simulation of an $Y_3Fe_5O_{12}$ rectangular thin film by applying the pulse magnetic field. We use the sample having a dimension of 15 μm×50 μm×1 μm, and the unit cell is 0.1 μm×0.1 μm×0.1 μm. The static magnetic field $\mathbf{H}_{dc}$=2.3 kOe is applied in the x direction. The Gaussian-shaped pulse field is also applied to the sample in the y direction with the amplitude 10 Oe and with the full width at half maximum (FWHM) 5 ps. We calculate time evolution for 100 ns after the pulse field is applied. The pulse field excites spin waves both magnetostatic backward volume modes (MSBVM) and magnetostatic surface waves (MSSW)[15]. Figure S2 shows the spatial distribution (x-y plane at (a), (b) z=0.5 μm and (c) z=1 μm) of the Fourier spectrum of the out-of-plane component (M_z) for the frequencies 6.5GHz, 6.8GHz and 7.1GHz. In contrast to the spin-wave spin current discussed in this article, the standing wave is excited because the spatially uniform field is applied. As shown in Figs. S2a and S2b, the wave vector in the x direction decreases with increasing the frequency. This negative dispersion indicates that the excited spin wave is the MSBVM. Figure S2c shows the spin wave at the surface layer where the spin wave of MSSW with a wave vector of the y direction is also excited. Due to the interference between the MSSW and the reflecting spin

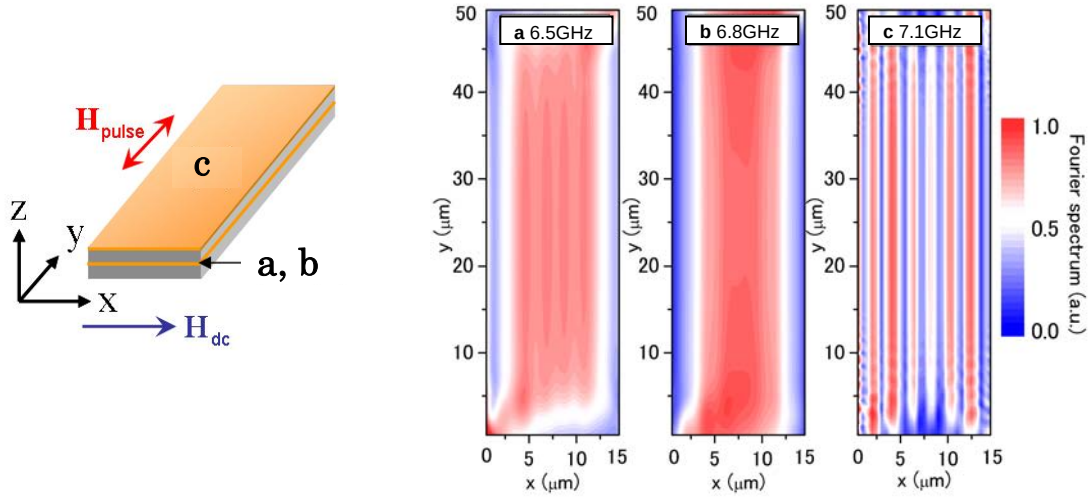

Figure S2: **a-c,** Spin waves in the rectangular thin film. Schematic picture shows the sample configuration. The Fourier spectra of out-of-plane component M_z at frequencies, (**a**) 6.5GHz, (**b**) 6.8GHz and (**c**) 7.1GHz are plotted, respectively. The spectra at the middle layer denoted in the configuration are shown in (**a**) and (**b**) and that at the surface layer in (**c**).

wave from the boundary, beating patterns in the *y* direction are observed.

Next, we show the numerical results of the spin dynamics excited by the spin Hall effect. We use the sample having a dimension of 7 mm×5 mm×1 μm with unit cell 10 μm×100 μm×0.1 μm. The static magnetic field $\mathbf{H}_{dc} = 2.3$ kOe is applied in the *x* direction. The Pt-film i covers the $Y_3Fe_5O_{12}$ film in the region *x*=0-5.5 mm. We consider the spin torque term $\boldsymbol{\tau}_{stt}$ due to the transmission of angular momentum from Pt-film i to $Y_3Fe_5O_{12}$ via an exchange interaction (see Supplementary Information, section B for details). The spin torque term is included by $\boldsymbol{\tau}_{stt} = c\,\mathbf{M}\times(\mathbf{s}\times\mathbf{M})$ in the right hand side of equation (S1), where **s** is the spin accumulation of the Pt-film i [39]. This torque acts on the surface layer attaching to the Pt-film i as shown in Fig. S3a. Parameter *c* is a magnitude of the spin torque which is proportional to the spin current $j_s(0)$ in equation (S15) through the interface between Pt-film i and $Y_3Fe_5O_{12}$ in the presence of

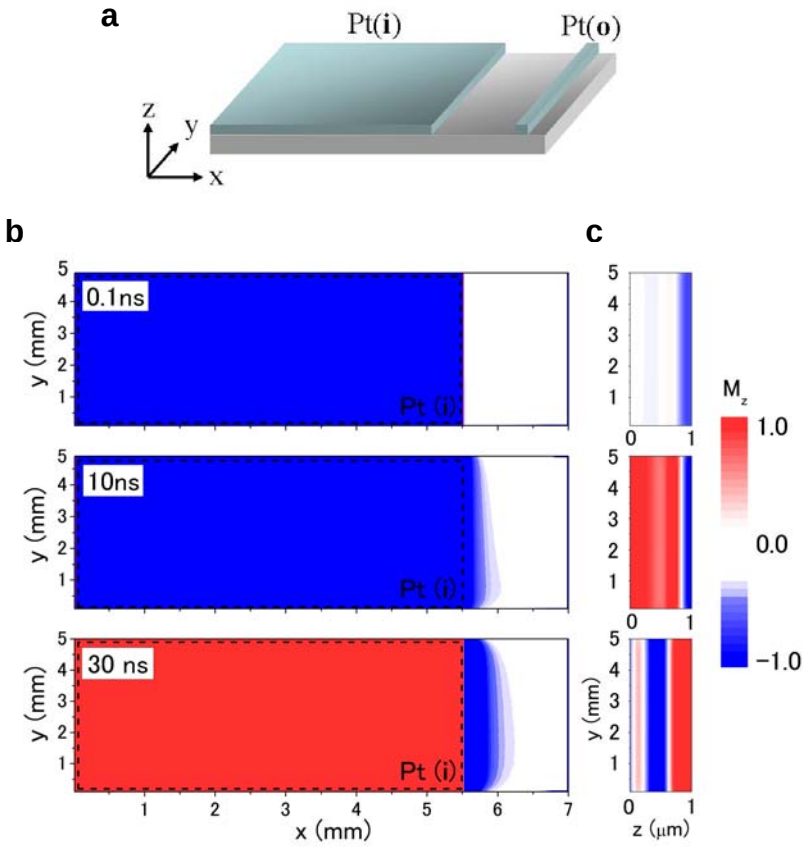

Figure S3: **a,** Sample geometry for calculating spin-wave spin current in $Y_3Fe_5O_{12}$. The Pt-film i exists in the region x=0-5.5 mm. The surface layer is taken to be z=1 μm. The torque term $\boldsymbol{\tau}_{int}$ exists at the surface layer where the Pt-film i is attached. **b,** Snapshots of the time evolution of the local magnetic moment at the surface layer. **c,** The local magnetic moment in the y-z plane at x=4 mm at time t=0.1, 10 and 30 ns.

the spin exchange interaction. When the static field $\mathbf{H}_{dc}$ is applied, the spin torque term $\boldsymbol{\tau}_{stt}$ points to the direction opposite to the damping vector $\mathbf{M}\times d\mathbf{M}/dt$. When the magnitude of $\boldsymbol{\tau}_{stt}$ is smaller than the damping vector, the magnetization relaxes to the minimum energy configuration after evaluating sufficiently long time. This situation is corresponding to that the charge current through Pt-film i is below the critical current. For obtaining the spin-wave spin current stationary, the parameter c is chosen so as that the magnitude is that of the damping term. In consequence of such a tuning of the parameter c, precession dynamics of

the magnetization is realized at the surface layer. We show a snapshot of the time evolution of the out-of-plane components of the magnetization in Fig. S2 at (b) the interface layer and (c) its cross section. At time t=0.1 ns, the precession mode is excited at the interface layer where the Pt-film i is attached. This precession mode excites spin waves propagating both in *x* and *z* directions. The spin waves propagating in the *z* direction is strongly affected by the shape anisotropic field of the thin film and reflected from the boundary. When the spin wave propagating in the *x* direction reaches to the position of Pt-film o, the magnetization dynamics induces the inverse spin Hall effect on Pt-film o, resulting an electric signal transmission. The spin-wave nonlinearity minimally affects this calculation since the calculation is done near the threshold excitation.

Additional References

32. Mills, D. L. & Rezende, S. M. Spin dynamics in ultrathin magnetic films, Spin dynamics in confined magnetic structures II, Hillebrands, B. & Ounadjela, K. (eds.), *Topics Applied Phys*. **87,** p. 27 (Springer-Verlag, Berlin Heidelberg, 2003).

33. Takahashi, S., Saitoh, E. & Maekawa, S. Spin current through a normal-metal/insulating-ferromagnet junction, *J. Phys.: Conf. Ser*. **200**, 062030 (2010)

34. Simanek, E. & Heinrich, B. Gilbert damping in magnetic multilayers. *Phys. Rev. B* **67,** 144418 (2003).

35. Mills, D. L. Ferromagnetic resonance relaxation in ultrathin metal films: The role of the conduction electrons. *Phys. Rev. B* **68,** 014419 (2003).

36. Zhang, S. & Li, Z. Roles of nonequilibrium conduction electrons on the magnetization dynamics of ferromagnets. *Phys. Rev. Lett.* **93,** 127204 (2003).

37. Heinrich, B., Fraitova, D. & Kambersky. V. The influence of s-d exchange on relaxation of magnons in metals. *Phys. Stat. Sol.* **23,** 501 (1967).

38. Tserkovnyak, Y., Brataas, A., Bauer, G. E. W. & Halperin, B. I. Nonlocal magnetization dynamics in ferromagnetic heterostructures. *Rev. Mod. Phys.* **77,** 1375 (2005).

39. Tserkovnyak, Y., Brataas, A. & Bauer, G. E. W. Spin pumping and magnetization dynamics in metallic multilayers. *Phys. Rev. B* **66,** 224403 (2002).